Surface Micromachined Microengine

ERNEST J. GARCIA and JEFFRY J. SNIEGOWSKI
Sandia National Laboratories, Albuquerque, NM, 87185 (U.S.A.)

Abstract

The design, fabrication, and preliminary testing of an electrostatically-driven polysilicon microengine is presented. This device has direct application as a drive and power source for micromachined mechanisms such as optical switches, electrical switches, micropositioners, or any other micro-sized device requiring mechanical power. This is the first device of its kind which is directly linked to an output gear and converts linear motion from comb-drive actuators to rotational motion. The microengine provides output in the form of a continuously rotating output gear (~50 microns in diameter) that is capable of delivering torque to a micromechanism. The microengine can be operated at varying speeds and its motion can be reversed. Processing considerations address the elimination of natural interferences that arise when conformally-deposited polysilicon films form the links, joints, and gears that comprise the microengine. The resultant device is completely batch fabricated without the need for piece-part assembly.

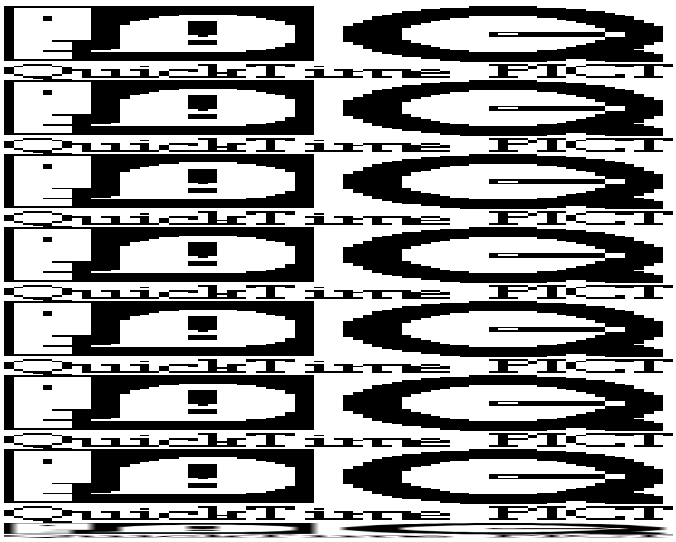

Fig. 1. SEM perspective view of the microengine output gear. Gear extreme diameter is approximately 50 microns.

Introduction

There exists a variety of instances where a power source is required to supply rotating mechanical motion to operate a micromechanism that is itself sized on the order of micrometers. Micromotors previously demonstrated [1,2,3] might be used if a means for power take-off can be demonstrated. In this work, however, we have taken the alternative approach of adapting an array of linear electrostatic comb actuators [4] to drive a rotating output gear [5]. Other types of linear actuators could also be used if sufficient force and displacement can be obtained.

An impact device which converts linear motion to rotary motion has been reported [6]. However, that device did not have a directly connected linkage to the rotary element, the rotation was not reversible, and the rotary element was not a gear, all of which are specific requirements for the microengine application. In short, the microengine was designed to serve in a similar fashion to a macroscopic-sized electric motor which has a myriad of applications in the macro world. In the microdomain, the microengine would serve as a general drive and power source to provide force and torque to drive micromechanisms.

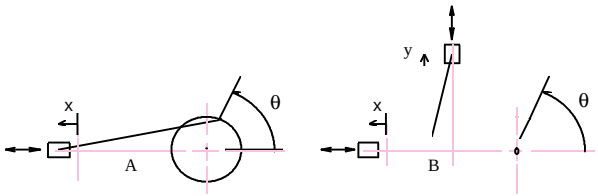

Fig. 2. Microengine schematic illustrating the principle of operation.

Figure 1 is a scanning electron micrograph of the output gear of the microengine. Fig. 2A illustrates the arrangement required to convert motion from a linear actuator into circular motion in the form of a rotating output element. The particular arrangement shown however, suffers from the problem of not delivering torque at $\theta = 0$ and 180°. This situation is analogous to that of a single piston engine. To remedy the problem, a flywheel is employed to maintain continuous motion. The concept of a flywheel can also be applied to the microengine, however, inertial effects are not useful during starting or at low speeds.

We have alleviated this problem altogether by introducing another drive linkage oriented 90° to the original linkage, shown in Fig. 2B. This second drive linkage, driven by another linear actuator, allows positive torque to be supplied to the output element throughout 360° of rotation. The second linear actuator must be operated 90° out of phase with the first actuator to produce synchronized motion of the output element, which in this case is a gear. The direction of rotation of the output gear is controlled

by either leading or lagging the input of the second actuator.

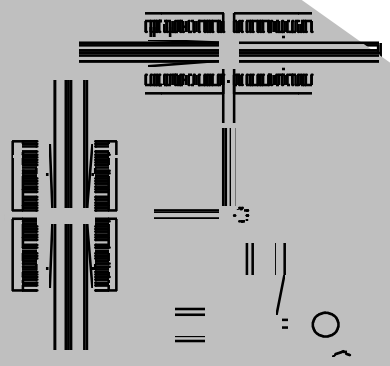

Fig. 3. Schematic drawing of the microengine relevant to actual physical layout of the device. Note: not shown is the second comb drive in series with those shown.

Fig. 3 illustrates the microengine arrangement with comb-drive actuators connected to the output gear by linkages. While Fig. 4 is an actual SEM of this arrangement. The linkages are connected to the actuators and output gear through pin joints that allow relative motion. The locations of the pin joints in Fig. 2B can be used as a reference to locate the pin joints in Fig. 3. The horizontal connecting link, also called the X drive link, is attached to the output gear through a pin joint at a radius of 17 microns relative to the center of the output gear. Fig. 3 shows this arrangement at $\theta = 0^{\circ}$ which is in the "as fabricated" position. Fig. 2 shows the configuration at some arbitrary angle θ. At $\theta = 0^{\circ}$, the X link will pass directly over the hub joint which supports the output gear. At this position it is possible that interference between the drive link and the output gear anchor joint will prevent the device from operating. Conformally deposited polysilicon will result in interference unless specific steps are taken to eliminate interference. The fabrication process which eliminates this interference will be discussed later. Note also that the actual microengine configuration uses two comb-drive actuators for both the X actuator and Y actuator for a total of four separate comb-drives. These additional comb-drives increase the available force for driving the system and the lateral stiffness of the system.

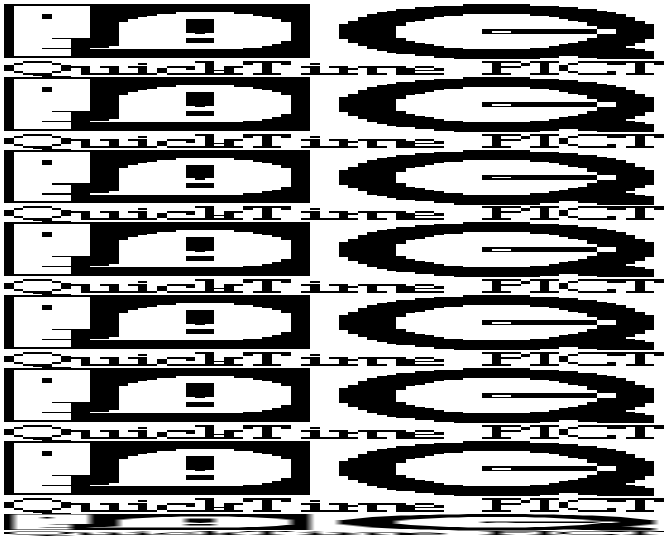

Fig. 4. SEM micrograph overview of the microengine.

Design

The design of the microengine requires that material, mechanical, electrical, and processing considerations are simultaneously addressed and synthesized. The following is a list of items that must be considered when designing micromechanical systems, and in particular, for the microengine.

-Size requirement of device

-Required displacements and speeds

-Required forces and torques

-Elastic material properties

-Frictional behavior

-Wear behavior

-Fatigue behavior

-Induced stresses

-Residual stresses

-Structural stiffness

-Structural stability

-Voltage induced deformations

-System kinematics and dynamics

-Processing limitations

-External interface and packaging

-Environmental conditions (temp, vibration,...)

-Cost

The geometry of the microengine (see Fig. 2) was explained in the introduction. Of prime importance is the requirement to deliver torque to the output gear at every position, i.e., from $\theta = 0$ to 360°. The arrangement with two input links allows for torque to be delivered at any position, and permits the device to

operate in clockwise or counterclockwise directions by proper phasing of the input forces.

The output gear for the microengine is connected to the X link through a pin joint at a radius of 17 microns (see Figure 2B). Therefore, the linear actuator driving the X link must be capable of a total motion equal to twice the joint radius, i.e., 34 microns, plus some allowance for clearances in the connecting joints. The X comb-drive actuator was designed to have a capability of 40 microns of total motion which allows for extra clearances in the joints. The Y comb-drive actuator requires less total motion capability since it is not directly connected to the output gear but is connected to the X-link at the position shown in Figure 3. Figure 5 shows the required X and Y comb-drive displacements for one configuration of the microengine. The total displacement required for the Y actuator is approximately 20 microns; however, the actual device was designed to have significantly more displacement to account for joint clearances, i.e., 40 µm total displacement.

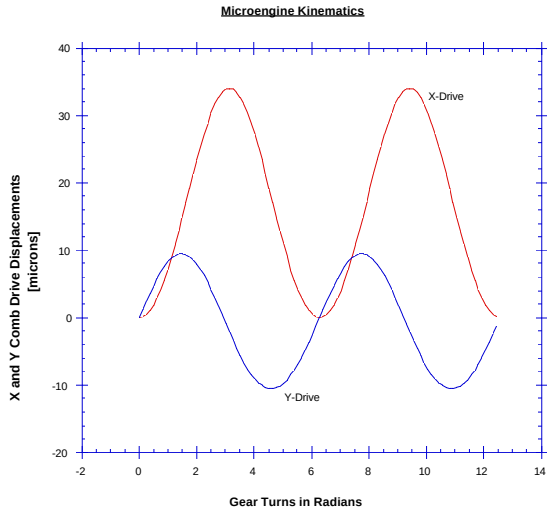

Fig. 5. Plot of the kinematic relation of gear position to linear actuator displacements.

For a frictionless system, this geometry can always deliver torque to the output gear. However, for a real system with joint and hub friction, there is a value of friction coefficient that will cause the machine to "lockup" and prevent the delivery of torque to the output gear. We would expect to be able to overcome the frictional force and deliver torque to a load, by simply increasing the output forces of the linear actuators . However, this is not the case. The friction force between two bodies in contact impedes their relative motion in the tangential direction and is directly proportional to the force normal to the direction of motion. Therefore, an increase in the normal driving force will result in a corresponding increase in the tangential friction force and the machine remains "locked up". Many macro-sized mechanical devices exhibit this behavior, e.g., machine screw jacks and geared transmissions. Because of the large scatter in friction data reported in the literature [7,8,9], we were concerned that "lockup" would be possible in the microengine, since some of the reported values were high enough to cause "lockup". One material configuration we chose to use in our joint system was silicon nitride on polysilicon. A joint system using polysilicon on polysilicon was also fabricated to compare with the performance of the silicon nitride material. The silicon nitride on polysilicon was superior to the polysilicon on polysilicon in air for both frictional and wear characteristics.

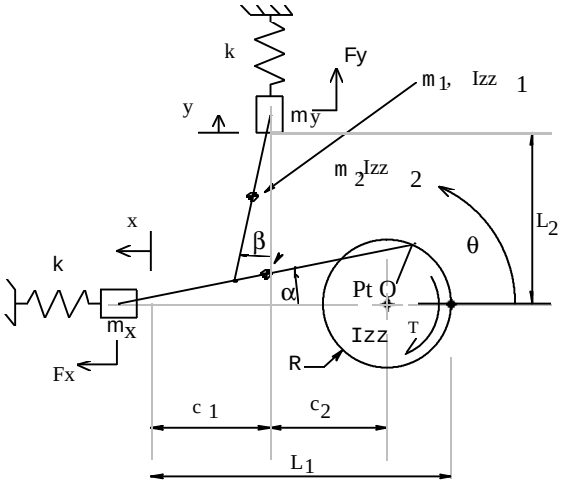

Fig. 6. Schematic illustrating the elements of the microengine configuration used in the mechanical model.

The dynamic analysis of the microengine begins with a definition of a system configuration and is a major part of the design iteration process. By combining, in part, results from succeeding dynamic analyses and other items listed earlier under design considerations, the system configuration evolves. Figure 6 defines the general configuration for the microengine and from this a mechanical model of the system is constructed.

The four equations below describe the kinematics of this single degree of freedom system and were used to generate the curves in Figure 5.

$$L_1 \cdot \sin(\alpha) = R \cdot \sin(\theta)$$
$$L_2 \cdot \sin(\beta) = x + c_1 \cdot (1 - \cos(\alpha))$$
$$x = L_1 \cdot (\cos(\alpha) - 1) + R \cdot (1 - \cos(\theta)) \qquad (1\text{-}4)$$
$$y = L_2 \cdot (\cos(\beta) - 1) + c_1 \cdot \sin(\alpha)$$

The inputs to this system are forces generated by the X and Y actuators. As mentioned earlier, a proper sequencing of X and Y input forces is required to generate an output torque in the desired direction. Figure 7 shows a combination of input force signals that will produce torque and motion at the output gear.

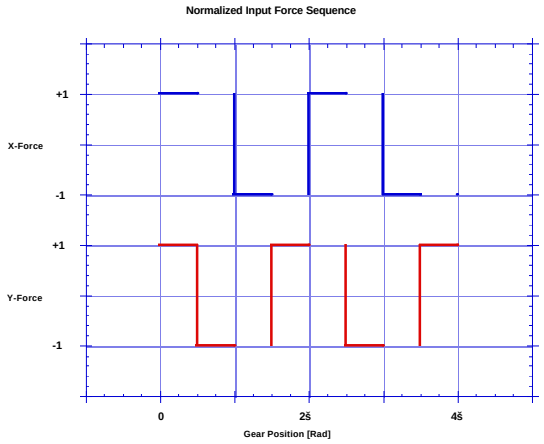

Fig. 7. The two offset square waves shown are an example of a simple drive signal set which successfully operated the microengine. The signals are normalized and have a phase shift of 90°.

Two types of analyses were carried out in the design sequence:

-Quasi-static case, with zero friction, to determine torque output as a function of angle θ for force inputs given in Figure 7

-Full dynamic system response, with friction and damping, for constant load torque T_{load}, and force inputs given in Figure 7

One method for deriving the equation of motion for the microengine is to use Lagrange's equations. For a single degree of freedom system the equation is,

$$\frac{d}{dt}\left(\frac{\partial K}{\partial \dot{\theta}}\right) - \frac{\partial K}{\partial \theta} + \frac{\partial V}{\partial \theta} = F_\theta \qquad (5)$$

where K and V are the kinetic and potential energies and F_θ is the generalized force. The first two terms in eqn. (5) are the inertia terms for the system and are determined from the masses, inertias, and angular and linear velocities of the system elements. Equations (1-4) are used, along with mass and inertia values for the system elements, to compute the kinetic energy K of the system. The inertia terms are then calculated using the first two terms in eqn. (5). The third term is the contribution due to system stiffness and is associated with the comb-drive actuator spring elements. The last term contains the contributions to the equation of motion from actuator input forces, damping, and friction effects in the system. Rewriting eqn. (5) so the inertia terms are on the left side we obtain,

$$\frac{d}{dt}\left(\frac{\partial K}{\partial \dot{\theta}}\right) - \frac{\partial K}{\partial \theta} = F_\theta - \frac{\partial V}{\partial \theta} \qquad (6)$$

The terms on the right hand side of eqn. (6) are the contributions to the equation of motion due to the X actuator input force F_X, the Y actuator input force F_Y, the load torque T_{load}, X actuator stiffness k_X, Y actuator stiffness k_Y, and the friction and damping generalized forces. Eqn. (7) gives the expression for the non inertial terms in eqn.. (6).

$$F_\theta - \frac{\partial V}{\partial \theta} = F_x \cdot R \cdot (\sin(\theta) - \cos(\theta) \cdot \tan(\alpha))$$
$$+ F_y \cdot R \cdot \left(-\tan(\beta)(\sin(\theta) - \cos(\theta)\tan(\alpha)) + \frac{c_1}{L_1} \cdot \cos(\theta) \cdot (1 - \tan(\alpha)\tan(\beta)) \right)$$
$$- T_{load} - F_{friction}(\theta, \dot{\theta}, \ddot{\theta}) - F_{damping}(\theta, \dot{\theta})$$
$$- k_{xcomb} \cdot x \cdot R \cdot (\sin(\theta) - \tan(\alpha)\cos(\theta))$$
$$- k_{ycomb} \cdot y \cdot R \cdot \left(\frac{c_1}{L_1} \cdot \cos(\theta) - \tan(\beta) \cdot (\sin(\theta) - \tan(\alpha)\cos(\theta) \cdot (1 - \frac{c_1}{L_1}))\right), \qquad (7)$$

For the quasi-static analysis case, the inertia terms are assumed to be approximately zero, and the friction and damping terms are neglected. The quasi-static equation of motion is now rearranged, the load torque T_{load} becomes the output torque T_{output}, and eqn. (7) is solved for T_{output}.

$$T_{output} = F_x \cdot R \cdot (\sin(\theta) - \cos(\theta) \cdot \tan(\alpha))$$
$$+ F_y \cdot R \cdot \left(-\tan(\beta)(\sin(\theta) - \cos(\theta)\tan(\alpha)) + \frac{c_1}{L_1} \cdot \cos(\theta) \cdot (1 - \tan(\alpha)\tan(\beta)) \right)$$
$$- k_{xcomb} \cdot x \cdot R \cdot (\sin(\theta) - \tan(\alpha)\cos(\theta))$$
$$- k_{ycomb} \cdot y \cdot R \cdot \left(\frac{c_1}{L_1} \cdot \cos(\theta) - \tan(\beta) \cdot (\sin(\theta) - \tan(\alpha)\cos(\theta) \cdot (1 - \frac{c_1}{L_1}))\right), \qquad (8)$$

From eqn. (8), the contribution to the output torque due to F_X and F_Y, as well as the effect of the system stiffness on the output torque T_{output}, can be readily evaluated. Figure 8 is a plot of the contribution of the X and Y actuators to the output torque. Here it can be seen that for each individual actuator there are regions where the output torque will be equal to zero. The addition of the torques due to both the X and Y actuators then assures that a non-

zero output torque is achieved for the actuator contributions at any angle. Also note that the Y actuator contribution to output torque is less than that of the X actuator. This is due to the offset of the Y actuator connection on the X link (Figure 2B). Equal torque contribution for the Y actuator would occur if the Y linkage was directly connected to the output gear joint at the same point as the X link is connected to the output gear. Gear/link clearance problems preclude placement of the Y link to eliminate the offset. Lengthening the X link, however, improves

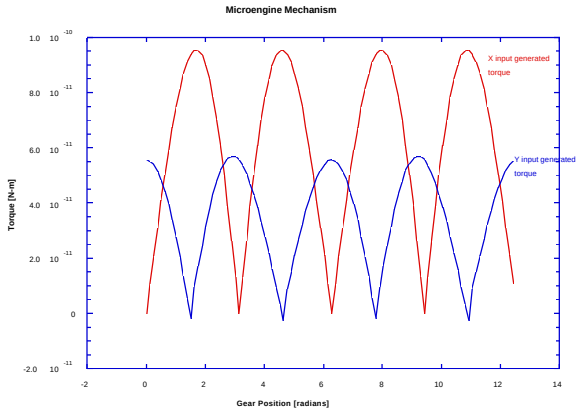

Fig. 8. Plot of the output torque due to X and Y actuator input forces.

The contribution of the actuator spring elements to output torque can also be determined from eqn. (8) and is given in Figure 9. The spring elements can either add to, or subtract from, the output torque depending on output gear angular position.

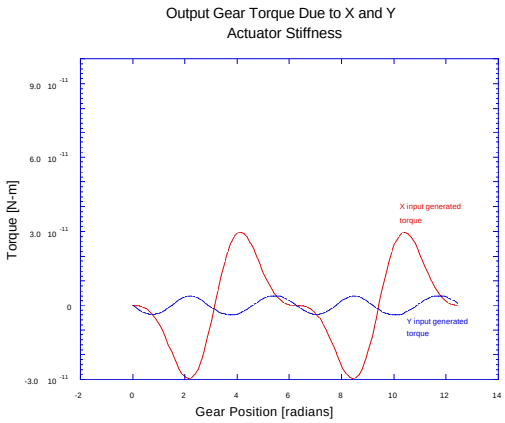

Fig. 9. Plot of the output torque due to X and Y actuator stiffness.

The total contribution to output torque is then the contribution of the X and Y actuator forces to output torque, and the contribution due to X and Y actuator stiffness. The total output torque is therefore described by all the terms in eqn. (8) and is given in

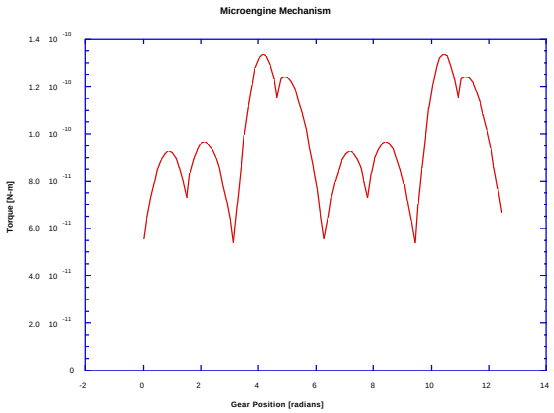

Fig. 10. Plot of the net microengine output torque

The results of Figure 10 show that a positive drive torque is obtained through a full rotation of the output gear. Recall this is the torque for the square wave actuator inputs given in Figure 7. Torque output for these particular actuator inputs is not constant with output gear position angle. This brings up the following question: Is there a set of inputs that would give a constant output torque? Manipulation of eqn. (8) shows that there are inputs that can result in a nearly constant torque through a complete revolution of the output gear.

The next logical extension to the quasi-static analysis would be to include the inertia terms in the equation of motion and compute the system response. In this case, we assume a constant load torque and solve the resulting equation of motion.

The derived equation of motion contains a large number of terms and is nonlinear; in fact, the inertia terms derived from eqn. (6) resulted in approximately 700 terms. The generation of these terms required the use of a symbolic equation manipulation program [10]. Expressions for damping depend on velocities of individual subelements and can be readily obtained by analytical expressions. However, closed-form expressions for generalized forces dependent on Coulomb friction in the system are not easily obtained since they introduce additional nonlinear algebraic equations that cannot be solved analytically. This occurs when the system becomes only moderately complex. Since friction is a major factor in the microengine mechanism, we cannot ignore it for this design and must resort to numerical dynamic solution codes which permit inclusion of Coulomb friction into the model [11].

Dynamic analyses of the microengine, which included effects due to damping [12,13] and Coulomb friction, was completed for several configurations of the microengine. Figure 11 shows the response of the microengine to 5 μN square wave inputs similar to those given in Figure 7 for ambient air conditions, using a static friction coefficient μ equal to 0.7, and

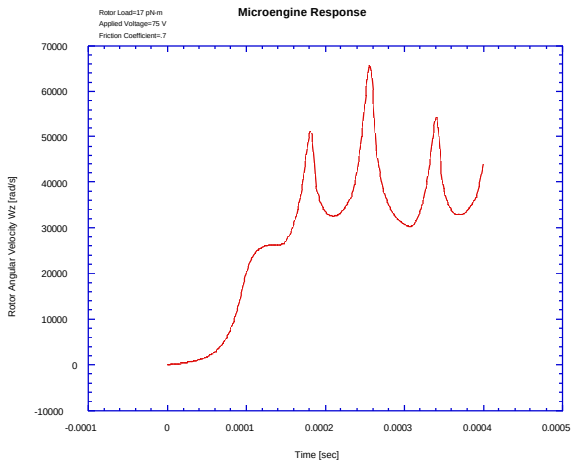

Fig. 11. Plot of the output gear angular velocity.

The analysis reveals that the microengine is capable of very high angular velocities. Note that 10,000 rad/s is approximately 100,000 rev/min. The variation in angular velocity is not surprising given the quasi-static results for output torque in Figure 10. It is interesting to note from Figure 11 that the average power output of the device can be estimated as $P=\omega \cdot T = 40{,}000$ rad/s 17 x 10^{-12}N-m Å 0.7 μW.

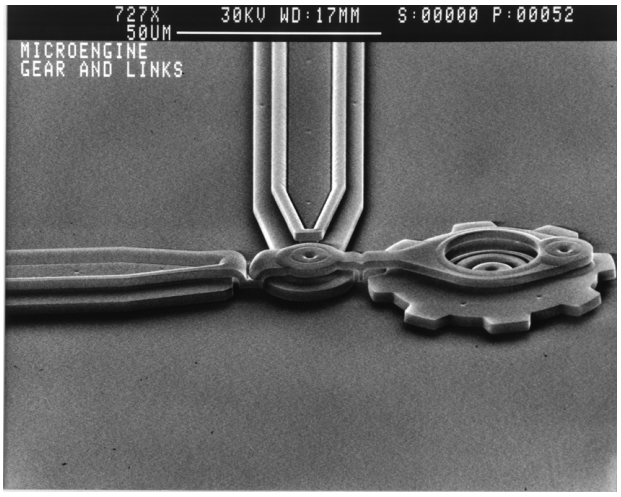

Fig. 12. SEM of a microengine design variation which has pin joints at all joint locations.

A conservative value of friction coefficient was chosen for the initial design analyses. As mentioned earlier, we were concerned about "friction lockup". Depending on the load torque, for values of μ starting between 0.9 and 1.2, "lockup" is experienced in the model. Preliminary test results on actual devices now lead us to believe the actual friction coefficient is between 0.3 and 0.4. For the microengine the sources of friction are in the pin joints, i.e., joints where the drive links connect to the actuators and output gear, and the main hub which anchors the output gear to the substrate. The design of the microengine shown in Figure 12 uses 5 pin joints.

We have also explored the use of flex joints which can be used when joint rotations are small. Figure 13 shows such a configuration where three of the joints in Figure 12, those that only move through a small angle, are replaced with flex joints. The use of flex joints then eliminates the frictional contribution of the pin joints, but adds additional stiffness to the system which can be undesirable. The buckling strength of the flex joints must also be considered when selecting flex joints over pin joints.

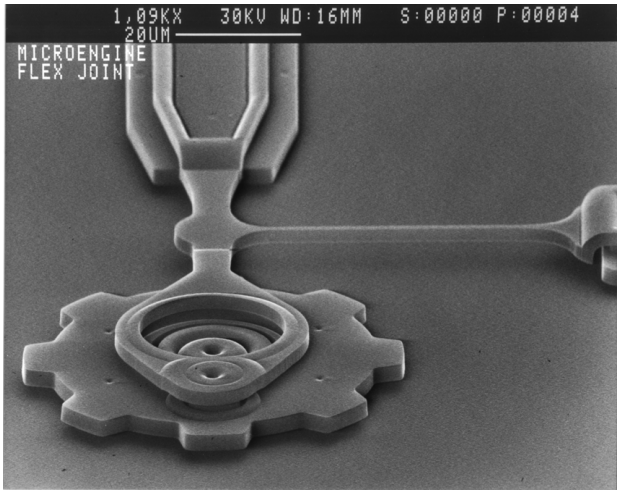

Fig. 13. SEM of a microengine design variation in which flex joints have replaced pin joints at joint locations with small angular displacements. Note: all joint locations, except for the connection to the gear, qualify for flex joint replacement.

Earlier a question was posed about making the output torque equal to a constant. Figure 10 shows the quasi-static output torque given by eqn. (8). Figure 11, for the dynamic case, shows that the angular velocity of the output gear varies while driving a constant load torque. The next logical question is: When driving the system at a constant torque, can the input forces be varied to yield a constant output gear angular velocity? The ability to deliver a constant angular velocity would be considered a valuable attribute of the microengine. To vary the input forces appropriately to obtain constant angular velocity would require the use of a feedback control system.

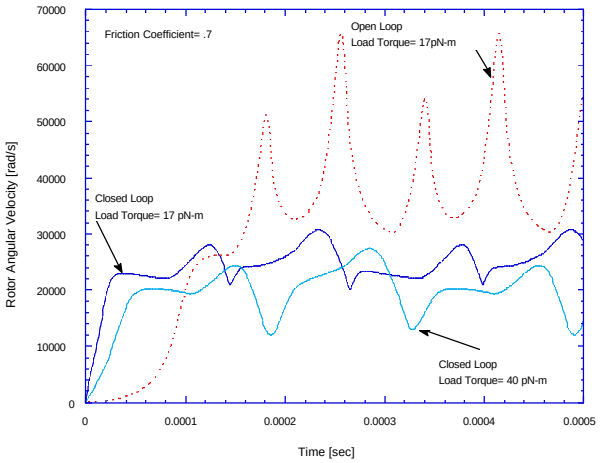

Fig. 14. Plot of the microengine response with feedbacl control.

Dynamic simulations of the microengine systen using both proportional and integral feedback contro were conducted. Figure 14 shows the response of th microengine to a simple proportional feedback contro scheme. Here the desired angular velocity is 25,00(rad/s driving a constant load torque of 17 pN-m. *A* separate curve on the same figure shows the results o feedback control when driving a 40 pN-m load torque at a desired angular velocity of 20,000 rad/s. The addition of proportional plus integral control further improves the response. To apply feedback control, a means for position determination is required. One method would be to measure capacitance changes in the actuators due to their changes in displacements. Another technique might use optical sensing of position, either externally or on-chip. The use of either of these methods could provide a strong motivation for having integrated electronics with the microengine structures.

For this analysis, the forces applied to drive the system are approximately 5 µN in magnitude and sequenced as in Figure 7. Also, of interest is the value of forces in the joints during operation of the microengine. We would expect for a quasi-static situation that the maximum forces in the joints would be of the order of 7 µN as in eqn. (9).

$$F_{Jo\ int_{Max}} \cong \sqrt{F_x^2 + F_y^2} \qquad (9)$$

This maximum force multiplied by the output gear joint radius (17 µm) gives values for torque very close to values given in Figure 10. From the dynamic analysis, however, we find that the maximum forces in the joints are 6-7 times the quasi-static value. Figure 15 shows the magnitude of the force in the joint where the X link connects to the output gear. These results indicate that the microengine behaves like macroscopic "high speed machinery" where dynamic forces are important. This pulsing of the forces in the joints will have important effects on the long-term wear and frictional properties of the joints. It is also interesting to note that for the cases where feedback control is used, the variation in joint forces

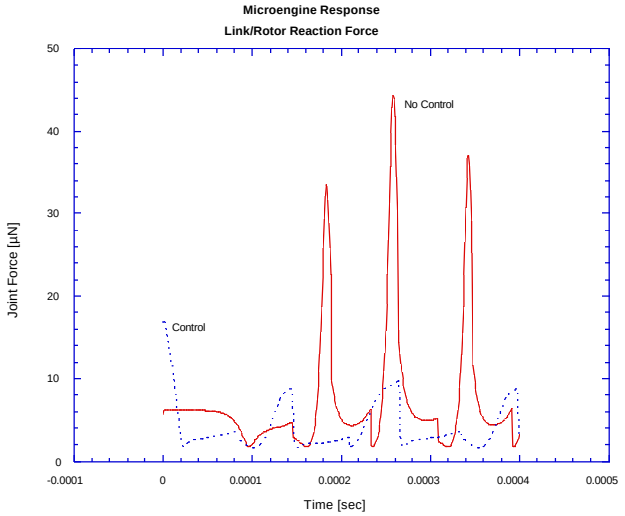

Fig. 15. Plot of the joint reaction forces.

Another item deserving comment concerns the nonlinearity of the equation of motion for the microengine system. Questions have been raised about the "natural frequency" of the system. The comb-drive actuators used in the system do have a natural frequency of vibration that is readily calculated. However, when they are connected into the microengine mechanism, the system is no longer linear and does not have a natural frequency of vibration that can be interpreted in the same way as that of a linear system. If a constant force is applied by the actuators in the X and Y directions, designated as F_x and F_y, the system will move to some equilibrium position θ_{eq}. A disturbance applied to the system in equilibrium will result in an oscillation of the system about the equilibrium position with a frequency which is dependent on the equilibrium position. For example, from numerical simulations, disturbances about an angle of $\theta = 140°$ result in an oscillation of the system at approximately 3300 Hz. This can be compared with disturbances about an angle of $\theta = 45°$, which results in oscillations at Å 1700 Hz. Individual subelements of the system will, however, have natural frequencies of vibration, e.g., comb teeth cantilevers. These natural frequencies must be examined to determine if microengine operating speeds could excite them to produce undesirable results, i.e., excessive deformations which interfere with the operation of the microengine.

It should also be
which is being driven
possesses inertia which mu
modelling the entire system.

The design of micromechanical syste
the microengine requires that the list of item
earlier be considered nearly in parallel with spec
attention to fabrication limitations. A sequence of iterations is used to revise the design based on modelling and testing results so that all requirements can be met. Two important items from the list- cost, and interfacing and packaging,- have not been addressed. Other design issues that are unresolved include the long-term wear and fatigue behavior of the system, and responses to temperature, vibration, shock, and other environments. These will lend themselves to detailed discussion when the appropriate testing is completed.

Fabrication

The entire microengine is fabricated of polysilicon on one wafer using surface micromachining batch fabrication techniques which are well known in the art [14]. The process for the described device does not rely on assembly of separately fabricated piece-parts, but is a fully batch-fabricated microengine. A linkage system which connected two rotary devices together has been demonstrated[15]. However, the links and rotary elements were originally fabricated on separate wafers which were then bonded together. The final structures were then realized by dissolution of one of the wafers. Operation of the linkages with manual probe manipulation was reported.

The fabrication of integrated gear-link assemblies by surface micromachining techniques presents several fundamental difficulties. In general, these difficulties are due to the vertical topology introduced by the deposition and etching of the various films used. Link/gear interference, which occurs with normally deposited films used in surface micromachining, has been alleviated by the present microengine design and fabrication process. This interference normally arises when the interconnecting link must pass over the gear edge, or the concentric retaining hub of the gear, as the mechanism moves through one complete rotational cycle.

Using an 8-mask process, the microengine can be produced in a way that avoids these difficulties. Non-interfering rotary motion of the system can be accomplished by a unique positioning and layout of the links, gear hub, and gear during the patterning and etching of these films. Upon final sacrificial etch and release, these considerations assure that full rotation is accomplished without interference.

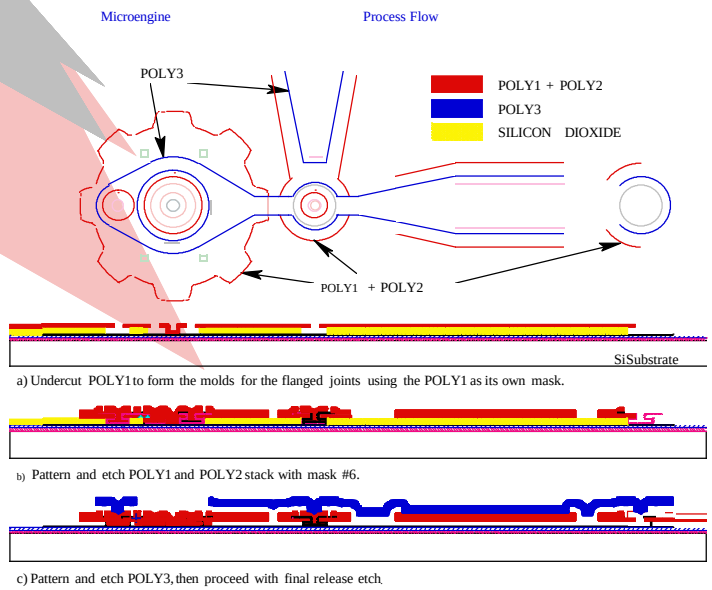

Fig. 16 Schematic cross-sections through essential elements of the gear and joints taken at three levels of device completion.

The microengine is formed using surface micromachining of multiple polysilicon films with intervening sacrificial oxide films. The fabrication of the microengine, including the electrostatic comb-drives, the power output gear, and the interconnecting linkages, requires four depositions of polysilicon. The first of the polysilicon layers serves to provide a voltage reference plane and electrical interconnect, while the remaining three polysilicon layers serve to form the mechanical elements. The electrical polysilicon is referred to as POLY 0, and the first, second, and third mechanical polysilicon films are referred to as POLY 1, POLY 2, and POLY 3, respectively. All polysilicon depositions are LPCVD, fine-grained polycrystalline silicon deposited at 580 °C.

To begin, a silicon substrate is coated with dielectric isolation films of Low Pressure Chemical Vapor Deposited (LPCVD) silicon-rich nitride over thermal oxide as a blanket starting point. The reason for the blanket isolation films is to ensure that proper electrical isolation is achieved between electrically active parts of the microengine structures.

The first patterned layer (which uses mask #1) is the electrical interconnect and shield polysilicon, POLY 0. The electrostatic comb-drive stator-to-substrate anchor areas and the stiction reduction dimple molds are patterned into the first thick sacrificial glass layer deposited after POLY 0, with masks #2 and #3, respectively. The subsequent polysilicon film to be deposited fills in the anchor and mold areas to provide attachment of the structures to

the substrate and 'dimples' on the otherwise flat underside of the polysilicon for stiction reduction.

The comb-drives and output gear are constructed from the first and second layers of mechanical polysilicon (POLY 1 and POLY 2), while the X and Y interconnecting link is formed from a composition of all three mechanical polysilicon films. The top view (Fig. 16) of the microengine has the polysilicon layers indicated for each of these elements. Sacrificial glass layers are used between the four polysilicon levels.

The flanged restraining hub for the output gear is formed from the POLY 2 deposition with the hub anchor being formed by a process in which the POLY 1 level is deposited and etched with mask #4 (see Fig. 16). Partial undercut etch of the sacrificial glass under POLY 1 is done to begin to form the basis for the flanged hub. The hub joint and link connections to the comb-drives and the output gear are of the flanged type and are formed by a process similar to and described in reference [16] (see Fig. 16b).

The partial undercut is backfilled by a thin (²0.5 µm) oxide deposition to form the spacing between the flange and the gear and link joints. This oxide is patterned by mask #5 to remain only in the joint and bearing areas. At this point, the POLY 2 deposition is done. The polysilicon deposition is conformal meaning that it uniformly coats any surface including backfilling the flange undercut. In the areas outside the joints and bearing where the flange spacer oxide was removed, the POLY 2 deposits directly on POLY 1 to form a single layer of polysilicon. This single layer comprises the gear body, parts of the links, and the comb-drives. The polysilicon sandwich is patterned and etched using mask #6 to form the above parts.

This sequence of depositions and critical dimensions outlined in the design rules produces nearly planar surfaces over the gear and joints. This permits non-interference of the gear/link assembly during operation. In addition, a silicon nitride friction-reduction layer is incorporated before the POLY 2 deposition to form a friction reduction layer on the flanged surfaces. This layer is illustrated as the solid black layer in Fig. 16b-c.

After the definition with mask #6, the second major sacrificial glass is deposited to a thickness on the order of 2 µm. Mask #7 is used to define the anchor areas for POLY 3 to the links and connecting flanged pin joint in the gear. The final POLY 3 layer is deposited, patterned, and etched using mask #8 to form the final link portions to connect the entire assembly. Note: if necessary, an additional mask #9 may be necessary to remove an artifact of the topology created during the anisotropic etch of POLY 3 known as stringers.

A cross-section just prior to the final release presents an overview of all the polysilicon and sacrificial films used (Fig. 16.b). A final hydrofluoric acid (HF) release etch produces the completed microengine assembly as shown in Fig. 16.c.

At two intermediate steps, namely after the POLY 2 and POLY 3 depositions, suitable post-deposition anneals must be done to assure that the polysilicon mechanical films do not display undesirable internal stress that would distort the structure upon the final release etch.

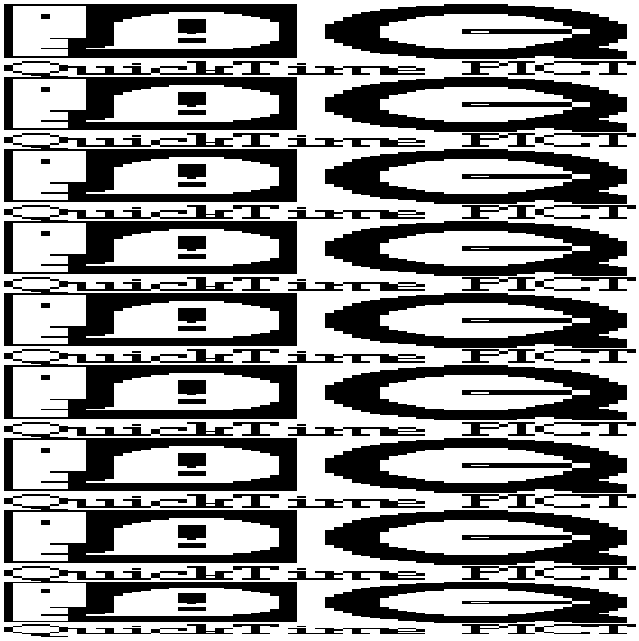

Fig. 17. A FIB micrograph of the cross-section of the gear, joint, and link area. This does not include the upper link formed from POLY 3 for clarity.

Figures 17, 18, and 19 are focused ion beam (FIB) micrographs of output-gear and pin-joint cross-sections. The cross-section details of the as-fabricated gear/link area are shown in the FIB micrograph image of Fig. 17. Fig. 17 is the cross-section before the final POLY 3 is included while Fig. 18 is just prior to the final release etch.

Fig. 18. Micrograph taken just prior to the final HF release etch and corresponding to the schematic process cross-section in Fig. 16.

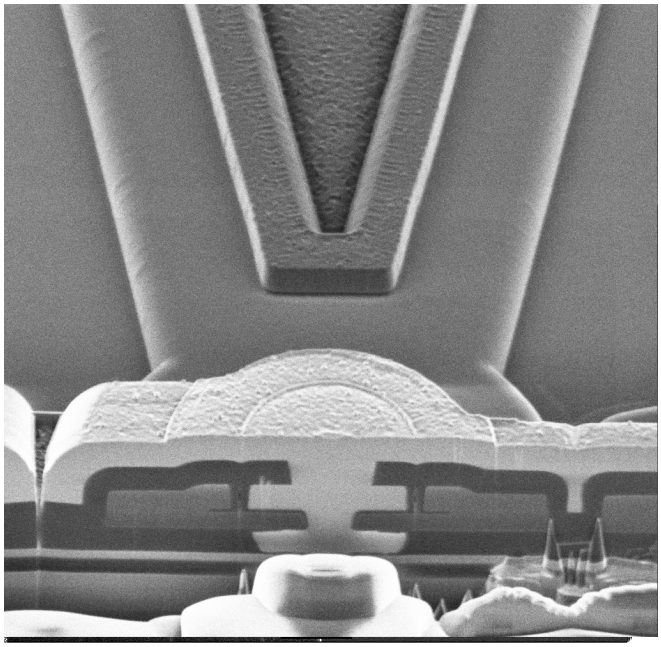

Fig. 19. Pin joint FIB cross-section.

Results

To date, several variations of the microengine design have been fabricated and initial testing started. Microengine design variations include:

-Linkage length variations

-Joint type variations; pin versus flex

-Joint clearance variations; 1000Å, 5000Å

-Joint material combinations;

silicon-on-silicon, and nitride-on-silicon joints

-Actuator stiffness variations; folding-beam

flexures and comb-teeth width

Preliminary testing of the microengine has been started, with the primary goal of demonstrating that full rotational motion of the microengine under its own actuation could be achieved. Other goals included: determining force levels required for sustained operation, maximum operating speeds, friction magnitudes, life cycle capability, and effects of other design variations on performance.

After final sacrificial oxide release, in several cases the final etch did not produce fully liberated structures due to surface tension induced stiction. One or more elements would slightly adhere to the substrate at the dimple locations on the structure. These stiction reduction dimples are used to prevent the structure from completely adhering to the substrate after final etch. Tapping the structure with a probe tip in one or more spots was required to release the devices for testing. There are suitable methods [17,18] for eliminating this effect and one of these methods will be incorporated in the process at a later date.

For the first microengine tests, complete rotating motion was achieved by the application of 25-35 V square wave inputs to the comb-drive actuators. These tests were performed in ambient air and full rotation was demonstrated. The initial tests were conducted using low frequency square waves as in Fig. 7. The motion observed was similar to that of a stepping motor. At application of the first signal, the output gear would move to an equilibrium position in the first quadrant, and remain in that position until the second set of signals was applied. The second set of signals would then move the output gear to an equilibrium position in the second quadrant, and so on until a complete revolution was obtained. Changing the phase relationship between X and Y actuators allowed for reversal of the microengine motion. Several devices were operated at square wave frequencies ranging from 0.5 Hz to 10,000 Hz (the upper limit of the particular test setup used). This represents output gear angular speeds ranging from 30 revolutions/min to 600,000 revolutions/minute. However, as the drive speeds are increased, there quickly comes a point where visual observations of the test device can no longer serve as verification that the device is moving as expected, i.e., at the frequency of the input drive signals. The use of high-speed video recording would be ideal for motion studies. We plan to use such a system in the future, but, for the present experiments, we relied on an optical fiber test to provide an independent measure of motion. A 25-µm optical fiber was used to pick up variations in the light reflected from a position where a drive linkage moves across the fiber's field of view. The reflected light variations picked up from the optical fiber are sensed by a photo diode whose output is amplified and displayed on an oscilloscope. Analysis of these signals can be used to verify full rotation of

the microengine at high speed. Detailed motion determinations will require the high speed video system mentioned above.

At voltages between 40 and 45 V, we observed that a single X comb-drive actuator tooth would deflect sufficiently to short with an opposing tooth of the stator. Another design variation of actuator resulted in a shorting voltage between 95 and 100 V. This shorting voltage depends on the stiffness of the actuator teeth, the stiffness of the actuator springs, the dielectric media, and the spacing between teeth. Electrostatic actuators experience a voltage induced elastic deformation in the teeth which leads to a stability problem. References [19, 20] describe a similar problem. At a given deformation, a tooth on the X actuator will snap through and short against the opposing tooth which also experiences a voltage induced deformation. This is due to the $1/(gap)^2$ voltage-induced force between teeth. In the microengine, the deformation comes from two sources: the deflection of the teeth under applied voltages, and the deflection of the entire X direction actuator and linkage. The latter is due to lateral loads applied on the X actuator by the Y direction actuators. During operation, as load torque increases, voltages must be increased to levels that provide sufficient forces to continue to drive the load. Consequently, as the voltages are increased, the above-mentioned deformations occur in the structure until the device shorts. This effectively defines the maximum torque limits of the microengine. Our modelling and experimental work in this regard is continuing.

Previously mentioned friction effects are of major importance in the system. Tests on a microengine with friction and viscous damping as its only loading-enabled estimation of friction coefficients. This was done by first modelling the system using various coefficients of friction, and then correlating those responses with experiments. This work is also preliminary, but led to the first estimate for coefficient of friction values (μ=0.3-0.4) given earlier.

Limited life-cycle tests were also conducted to determine how many operating cycles could be expected from the configurations chosen. One version of microengine, which had 5000 Å clearances in silicon-on-silicon joints, was run approximately 10^5 cycles before the operation required increased voltages for continued operation. Another version with similar clearances, but with approximately 1500 Å of silicon nitride on one side of the joints, was run 2.8×10^6 cycles before increased operating voltages were required. These tests were run in ambient air. Another test used a microengine with silicon-on-silicon joints, with 5000 Å clearances in the joints, but was run in 20 centistoke viscosity silicone oil. This test is not yet completed, but to date greater than 12×10^6 cycles have been run without any apparent degradation, i.e., without requiring increased operating voltages. This is, to our knowledge, the first time a true lubricating fluid has been used in the operation of a microactuator. These initial results clearly indicate the tribological benefits of a lubricating medium even at these dimensions. If operating conditions allow, the use of a lubricating medium such as silicone oil is advantageous.

As expected, silicon-on-silicon is a poor tribological combination in ambient air, and unless silicon-on-silicon is run with a lubricant, the use of other material combinations such as silicon nitride-on-silicon, or diamond-like carbon-on-silicon, etc., will certainly be required.

Evaluations which will look at the effects of clearance variations in the joints are pending.

Although these results are preliminary, they are very encouraging. Because of this early success, several additional topics for investigation will be pursued. As tests are completed, continuing reports will be made.

Conclusions

A surface micromachined microengine has been successfully designed, fabricated, and operated. This device is completely batch fabricated with all links, joints, gears, and other elements formed as part of the batch process. The extremely small size of this device permits output gear angular velocities of 600,000 rev/min to be achieved. Additional modelling indicates that even greater angular speed can be attained.

Many issues related to this design are only partially resolved. The preliminary success demonstrated, however, indicates that these issues are not insurmountable. We are continuing with our analyses and evaluations to better understand the microengine so that optimization of the design and fabrication of the microengine can be accomplished. We believe we are nearly in a position to use the microengine to drive the specific micromechanisms that provided the original motivation for developing this device.

Acknowledgment

The authors are grateful to D. Chavez, Silicon Technologies Dept., for her invaluable assistance in the fabrication of the microengine, M. Polosky, Electromechanical Components Dept., for testing

assistance, J. Rife and A. Campbell, Failure Analysis Dept., for their preparation of the FIB micrographs, P. Shea for preparation of SEM micrographs, and the staff of the Microelectronics Development Laboratory at Sandia.

References

[1] L-S. Fan, Y-C. Tai, and R. S. Muller, "IC-processed Electrostatic Micromotors", Sensors and Actuators, Vol. 20, 1989, pp. 41-47.

[2] Y-C. Tai and R. S. Muller, "IC-processed Electrostatic Synchronous Micromotors", Sensors and Actuators, Vol. 20, 1989, pp. 49-55.

[3] M. Mehregany, et. al., "Operation of Microfabricated Harmonic and Ordinary Side-Drive Motors", Proc. of Micro Electro Mechanical Systems, Napa Valley, CA, Feb. 1990, pp. 1-8.

[4] W. C. Tang, T-C. H. Nguyen, and R. T. Howe, "Laterally Driven Polysilicon Resonant Microstructures," Sensors and Actuators, vol. 20, 1989, pp. 25-32.

[5] E. J. Garcia and J. J. Sniegowski, "The Design and Modelling of a Comb-Drive-Based Microengine For Mechanism Drive Applications", Proceedings of the 7th International Conference on Solid-State Sensors and Actuators (Transducers '93), Yokohama, Japan. June 7-10 1993, pp 763-766.

[6] A. P. Lee and A. P. Pisano, "Polysilicon Angular Microvibromotors", J. of Microelectromechanical Systems, Vol. 1, No. 2, June 1992, pp. 70-76.

[7] Y-C. Tai and R. S. Muller, "Frictional Study of IC-processed Micromotors", Sensors and Actuators, vol. A21-A23, 1990, pp. 180-183.

[8] K. J. Gabriel, F. Behi, R. Mahadevan and M. Mehregany, "*In situ* Friction and Wear Measurements in Integrated Polysilicon Mechanisms", Sensors and Actuators, vol. A21-A23, 1990, pp. 184-188.

[9] K. Deng, W.H. Ko and G. Michal, "A Preliminary Study on Friction Measurements in MEMS", Tech Digest 6th Int. Conf. on Solid-State Sensors and Actuators, San Francisco, CA, June 1991, pp. 213-216.

[10] Wolfram Research, Champaign, IL, USA.

[11] CADSi, Coralville, IA, USA.

[12] Y-H. Cho, A. P. Pisano, and R. T. Howe, "Viscous Damping Model for Laterally Oscillating Microstructures", Journal of Microelectromechanical Systems, Vol. 3, No. 2, June 1994, pp. 81-87.

[13] X. Zhang and W. C. Tang, "Viscous Air Damping in Laterally Driven Microresonators", Proc. of Micro Electro Mechanical Systems, Oiso, Japan, Feb. 1994, pp. 199-204.

[14] R. T. Howe, "Surface Micromachining for Microsensors and Microactuators", J. Vac. Sci. Technol., Vol. B 6, pp. 1809-1813, 1988.

[15] Y. Gianchandani and K Najafi, "Batch Fabrication and Assembly of Micromotor-Driven Mechanisms with Multi-Level Linkages", micro Electro Mechanical Systems '92, Travemunde (Germany), Feb. 4-7, 1992.

[16] L-S. Fan, Y-C. Tai and R. S. Muller, "Integrated Movable Micromechanical Structures for Sensors and Actuators", IEEE Trans. Electron Devices, vol. 35, no. 6, June 1988, pp. 724-730.

[17] J. J. Sniegowski, "Design and Fabrication of the Polysilicon Resonating Beam Force Transducer", Ph.D. thesis, Chapter 4, University of Wisconsin, Nuclear Engineering and Physics Department, 1991.

[18] G. T. Mulhern, D. S. Soane, and R. T. Howe, "Supercritical Carbon Dioxide Drying of Microstructures", Proceedings of the 7th International Conference on Solid-State Sensors and Actuators (Transducers '93), Yokohama, Japan. June 7-10 1993, pp 296-298.

[19] P. Osterburg, et. al., "Self-Consistent Simulation and Modelling of Electrostatically Deformed Diaphragms", Proc. of Micro Electro Mechanical Systems, Oiso, Japan, Feb. 1994, pp. 28-32.

[20] L. Y. Chen, et. al., "Selective Chemical Vapor Deposition of Tungsten for Microdynamic Structures", Proc. of Micro Electro Mechanical Systems, Salt Lake City, UT, Feb. 1989, pp. 82-87.

This work was performed by Sandia National Laboratories, Albuquerque, New Mexico, 87185 for the United States Department of Energy under Contract DE-AC04-94AL85000.

Biographies

J. J. Sniegowski received his Ph.D. degree in Nuclear Engineering and Engineering Physics from the University of Wisconsin- Madison in 1991. He is a Senior Member of the Technical Staff in the Silicon Technologies Department at Sandia National Laboratories, New Mexico, USA. Dr. Sniegowski is responsible for leading the development of micromachining technology at the Microelectronics Development Laboratory at Sandia National Laboratories. His research interests include microactuation with micromechanisms, microsensors, and material science of thin films.

E J. Garcia received B.S. amd M.S. degrees in Mechanical Engineering from the University of New Mexico and the University of California, Berkeley. He is a Senior Member of the Technical Staff in the Electromechanical Components Department at Sandia National Laboratories, New Mexico, USA. His work is primarily concerned with precision machine design, with particular application to inertial sensing, and more recently, design of micromechanical systems. His most recent interests pertain to the dynamics of micromechaincal devices and systems, especially actuation devices. He is a Registered Professional Engineer, and a member of ASME, Tau Beta Pi, and Pi Tau Sigma.